Published in final edited form as:
Acad Radiol. 2012 July ; 19(7): 834–841. doi:10.1016/j.acra.2012.03.003.

MR Elastography in Renal Transplant Patients and Correlation with Renal Allograft Biopsy — A Feasibility Study

Christine U. Lee, M.D., Ph.D.*, **James F. Glockner, M.D., Ph.D.**, **Kevin J. Glaser, Ph.D.**, **Meng Yin, Ph.D.**, **Jun Chen, Ph.D.**, **Akira Kawashima, M.D., Ph.D.**, **Bohyun Kim, M.D., Ph.D.**, **Walter K. Kremers, Ph.D.**, **Richard L. Ehman, M.D.**, and **James M. Gloor, M.D.**
Department of Radiology (CUL, JFG, AK, BK, RLE), Center for Advanced Imaging Research (KJG, MY, JC), Department of Biostatistics (WKK), Department of Nephrology and Hypertension (JMG), Mayo Clinic, Rochester, MN, United States

Introduction

The incidence of renal allograft rejection has been considerably reduced by the introduction of immunosuppressive drugs. However, it remains difficult to optimize anti-rejection therapy for transplant recipients because of the lack of non-invasive biomarkers for rejection. Kidney transplant (KTx) biopsy with histopathologic examination is therefore frequently necessary to guide therapy in patients with diminishing renal function. Ultrasound-guided KTx biopsies for interval histopathologic assessment are obtained 4 months, 1 year, 2 years, and 5 years after transplantation at our institution. Due to strict criteria for tissue adequacy outlined by Banff'97 (1), an international schema developed in the early 1990's for classifying renal allograft pathology, three 18-guage core biopsy specimens are typically acquired, but the number of specimens can range from 1 (usually in the setting of an immediate complication) to 5. As would be expected, the value of this histopathologic gold-standard is heavily dependent on the biopsy specimen. Investigations on specimen inadequacy have been highly variable, with one study of 1171 biopsies reporting 23% inadequate biopsies using a 16-gauge device and 47% inadequate biopsies using an 18-gauge device (2), another study of 345 biopsies reporting 5.2% non-diagnostic biopsies using a 14-gauge biopsy device (3), and yet another study of 294 biopsies reporting only 5% inadequate biopsies using an 18-gauge device and a cortical tangential approach (4). The rate of major complications requiring additional intervention beyond observation, such as blood transfusion, surgery, or embolization for large perirenal hematomas,

*Corresponding author: Christine Lee, MD, PhD, Mayo Clinic, 200 First St, S.W., Rochester, MN 55905, 507 266 1207, 507, 266 1657 (Fax), lee.christine@mayo.edu.

Support and Financial Disclosure Declaration:
Christine U. Lee, M.D., Ph.D.* None
James F. Glockner, M.D., Ph.D. None
Kevin J. Glaser, Ph.D. NIH grant EB001981
Yin, Meng, Ph.D. NIH grant EB001981
Jun Chen, Ph.D. NIH grant EB001981
Akira Kawashima, M.D., Ph.D. None
Bohyun Kim, M.D., Ph.D. None
Walter K. Kremers, Ph.D. None
Richard L. Ehman, M.D. NIH grant EB001981
James M. Gloor, M.D. None

arteriovenous fistulas, or urinomas also varies greatly ranging from <1% to <3% (2–5). Loss of the allograft and death have also been described.

Magnetic resonance elastography (MRE) is a non-invasive, phase-contrast-based technique that images the propagation of mechanical shear waves in tissue and uses that information to generate quantitative measures of tissue stiffness in kilopascals. Hepatic MRE has been successfully performed in thousands of patients, including liver transplant recipients, where good correlation between histologic grade of fibrosis and tissue stiffness measured with MRE has been established (6). Recent investigations now suggest that changes in the viscoelastic properties of tissue may reflect derangements in the extracellular matrix which can be a harbinger of developing pathology (7).

KTx recipients are a well-defined patient population with an organ of interest that is ideally positioned for MRE as well as a routinely acquired histopathologic gold standard. Park et al have demonstrated that fibrosis with inflammation at one year is associated with not only reduced graft function and survival but also a rejection-like gene expression signature (8). The purpose of this investigation is to assess the feasibility of obtaining MRE data in KTxs and correlating this with biopsy results in a small group of patients.

Materials and Methods

Following approval by the Institutional Review Board and in accordance with the Health Insurance Portability and Accountability Act, eleven consecutive adult male or non-pregnant female KTx patients who were otherwise healthy and returning for their annual or post-annual protocol evaluation were recruited for the study. During the screening process, patients were excluded if there was any contraindication for MRI (including pacemakers, cochlear implants, and certain spinal stimulation devices), or if there was any procedure or event involving the KTx that may have required hospitalization or intervention within the prior six months. In the setting of multiple KTxs, the most recent, functioning renal allograft was targeted in this study.

Reproducibility of MRE measurements was assessed in one patient who returned for clinical follow up without biopsy. MRE was performed three consecutive times with removal of the patient from the magnet and repositioning of the MRE apparatus prior to each scan.

Imaging Technique

Immediately prior to the MRE exam, a targeted ultrasound examination was performed to localize the allograft, and skin markers were placed to guide placement of the surface coil and vibration plate. Each patient was positioned feet first and supine in a 3 Tesla MR scanner (Discovery MR750, GE Healthcare, Waukesha, WI) and imaged with an eight-channel receive-only torso phased array coil. After localizing the allograft, MRE acquisitions were performed using 90-, 120-, and 150-Hz vibrations and a flow-compensated, single-shot, spin-echo echo planar imaging multislice 2D MRE imaging sequence. Depending on the size of the patient and the position of the transplanted kidney, the imaging orientation was either axial or sagittal with the frequency-encoding direction right-left or superior-inferior, respectively. Other imaging parameters included field of view (FOV) = 32-40 cm, 96×96 acquisition matrix reconstructed to 128×128, parallel imaging acceleration factor of 3, 30–40 3-4-mm contiguous slices, (repetition time/echo time) TR/TE = 1700-1850/48-60 ms, and motion sensitivities of 23.4, 19.5, and 8.2 $\mu m/\pi$ radians for the 90-, 120-, and 150-Hz acquisitions, respectively. For each frequency of motion, four time points of the motion and all three directions of the vector motion were sampled. The acquisition time was 1.75-2 minutes and the acquisitions were performed with free breathing. MRE scout images were obtained in both axial and sagittal planes.

The mechanical vibrations required for the MRE exams were supplied by an active pneumatic driver system located outside of the scan room (Resoundant, Rochester, MN) and were conducted into the scanner bore via a ¾-inch diameter, 24-ft long, plastic tube in a manner similar to Yin et al. (9) The tube terminated in a soft, pillow-like, passive actuator (10) that was placed over the renal allograft using the skin marker for guidance. The passive actuator was approximately 3×3 inches and consisted of a soft, inelastic fabric cover around a porous, springy, mesh core which prevents the driver from collapsing even under load. The passive actuator was supplied by a 15-inch long, 0.5-inch diameter plastic tube that was connected to the main tube from the active driver (Figure 1). The passive actuator was held in place against the body wall of the patient via an elastic belt that was wrapped around the patient. MRE was then performed either in the axial or sagittal plane (Figure 2) based on which plane of acquisition yielded greater cortical thickness.

Data Analysis

The renal tissue stiffness was calculated in an identical manner for each frequency of motion. The first temporal harmonic of the vector curl of the measured wave field was calculated to reduce artifacts caused by the presence of longitudinal wave motion, boundary effects, and static phase errors. This was done using 3×3×3 pixel windows and an algorithm that did not require unwrapping the measured phase data (11). The curl of the displacement data was then inverted using a 3×3×3 direct inversion (DI) algorithm incorporating 20 3D directional filters (DF) with a 4^{th}-order Butterworth radial bandpass filter component with cutoff frequencies of 0.001 and 40 cycles/FOV (12). The renal parenchyma was manually segmented excluding the hilar region for each slice. The stiffness was then determined for the entire segmented renal volume by taking the average of all slices. Histograms of the tissue stiffness at the three difference frequencies for one patient are shown in Figure 3.

Pathology

All patients underwent clinically indicated ultrasound-guided protocol core-needle KTx biopsies All pathology reports included not only the Banff scores (13) but also diagnostic comments on the degree of interstitial fibrosis. These results were collected and reviewed in conjunction with the MRE data.

Results

Of the eleven patients recruited for this study, ten had protocol biopsies immediately following MRE, and one had KTx biopsy the day before MRE. The patient who had MRE after biopsy was excluded from the study. The mean age of the ten patients was 49.1 years ranging from 31–71 years; 6/10 (60%) were male. Lifetime number of KTx's was four for one patient and one for the remaining nine patients. One patient was scheduled for the first annual protocol biopsy; four patients for the 2-year protocol biopsy; one patient for a 4-year post-transplant biopsy; and, four patients for the 5-year protocol biopsy. Four patients had proliferative glomerulonephritis, three with IgA nephropathy and one with membranoproliferative glomerulonephritis. The remaining 6 patients had varying etiologies for renal failure: membranous glomerulonephritis, polycystic kidney disease, vesicoureteral reflux and chronic pyelonephritis, congenital hypoplastic kidney, radiation nephritis, and endstage renal failure due to diabetes mellitus type 2 and hypertension. Conceptually, vibrations generated during the MRE could pose risk (albeit very small) of vascular anastomotic dehiscence. Operative reports of all 10 patients described no vascular anastomotic complications during the operative or immediate post-operative period. Subsequent diagnostic ultrasounds of the anastomoses performed as part of post-operative care were also normal. Vital signs were obtained prior to MRE in 9/10 patients. Four patients were normotensive (systolic < 120 mmHg and diastolic <80 mmHg); 5 were

prehypertensive (systolic 120–139 mmHg or diastolic 80–89 mmHg); and, 1 was Stage 1 hypertensive (systolic 140–159 mmHg or diastolic 90-99 mmHg). Six of the 10 patients had moderate reductions in estimated glomerular filtration rates (eGFRs) as defined by the National Kidney Foundation; and the remaining four had severe reductions in eGFRs. Characteristics of the ten patients are summarized in Table 1.

Two of the ten patients were scanned in the axial plane, and 8/10 patients were scanned in the sagittal plane. Regardless of the plane of acquisition, the total scan time was approximately 20 minutes. All 10 patients were imaged using both 90- and 120-Hz vibrations, and the last 8 patients were imaged additionally with 150 Hz vibrations.

All patients underwent protocol core-needle biopsies: three core-needle biopsy passes were made on 8/10 patients and four passes were made on 2/10 patients. There were no immediate post-biopsy complications. At the time of pathologic evaluation, nine out of ten (90%) biopsies met the Banff criteria for tissue adequacy and were therefore diagnostic; one biopsy (10%) was inadequate and therefore non-diagnostic. Of the nine diagnostic biopsies, one had no significant fibrosis, six were diagnosed with mild interstitial fibrosis and tubular atrophy, and two were diagnosed with moderate interstitial fibrosis and tubular atrophy (Table 2). The pathologic diagnosis of “no significant fibrosis” was given when there were minimal findings, e.g., one or two atrophic tubules out of hundreds, which would translate to no clinical significance.

Table 3a illustrates the individual results of the calculated tissue stiffness with the degree of interstitial fibrosis. The sample sizes involved in this study were small and the power to detect differences between groups likewise small. The mean stiffness for the two cases with moderate interstitial fibrosis was higher than the mean of the six cases with mild interstitial fibrosis, but not significantly so (Hz 90, $p=0.12$; Hz 120, $p=0.17$; Hz 150 $p=0.26$). The mean stiffness of the two cases with moderate interstitial fibrosis was slightly greater than the mean of the one case with no interstitial fibrosis at 90 Hz but not significantly so ($p=0.78$) and slightly less at 120 and 150 Hz ($p=0.88$, $p=0.76$). Though smaller, the mean stiffness of the six cases with mild interstitial fibrosis did not differ significantly from the one case no interstitial fibrosis (Hz 90, $p=0.35$; Hz 120, $p=0.22$; Hz 150, $p=0.16$). These tests were made by comparing groups using a t-test within an ANOVA model. No corrections were made for multiple comparisons in these calculations. Boxplots of the mean tissue stiffness at all the frequencies of vibration (90 Hz, 120 Hz, and 150 Hz) corresponding to the pathology results are shown in Figure 4. The repeatability study performed on one of the study patients demonstrated a covariance of 2.9% at 90 Hz, 3.5% at 120 Hz, and 5.4% at 150 Hz (Table 3b).

Discussion

MRE has been applied to several organs in addition to the liver, including the spleen, brain, lung parenchyma, heart, and prostate (14–19). With minor modifications to the standard hepatic MRE protocol, this study has demonstrated the feasibility of performing MRE on KTxs. All patients tolerated the scans and were able to proceed to protocol biopsies. Given the very small sample size, clinical utility and significance based on correlation of pathology with calculated renal stiffness cannot be established in this study. A larger series is needed to investigate the potential for the elastography technique to eliminate some of the currently mandated transplant biopsies.

In this small-sample investigation there was a trend toward higher mean stiffness in patients with moderate fibrosis in comparison to those with mild fibrosis, although this difference did not reach statistical significance. Why KTxs with mild fibrosis might have a lower

stiffness compared to the one case with no significant fibrosis is uncertain; previous studies have shown that perfusion pressure profoundly affects the stiffness of the kidney (20–22). It is possible that renal stiffness measured by MRE represents a combination of a static component reflecting the stiffness of the parenchyma itself which is hypothesized to be increased by fibrosis, as well as an additive dynamic component representing the hydrostatic swelling effect of perfusion pressure. Perhaps for the case with no significant fibrosis, the KTx was able to achieve higher hydrostatic pressure resulting in higher stiffness values. In this study, no association could be made between fibrosis and the use of calcineurin inhibitors as well as angiotensin-converting enzyme inhibitors. Successfully separating the effect of fibrosis from the confounding effect of hemodynamic variables (e.g. hydration state, perfusion pressure) at any given time is an area of active investigation (23). While no associations could be made in this investigation between blood pressures and stiffness values, given the small number of patients, blood pressure and perfusion effects reflected by renal artery and renal vein blood flow could also be measured by MRI and may help to distinguish different effects contributing to measured renal stiffness.

In the MRE data analysis, the segmented renal parenchyma included both cortex and medulla which could be a source of error since pathological evaluation is valid only on renal cortex and not medulla. Initial attempts to segment only the cortex yielded inadequate wave information for stiffness calculation as the average thickness of the renal cortex is approximately 6 mm (24), which is only about 2 voxels at the current image resolution. Therefore, partial volume effects between the cortex and medulla exist in the MRE data. Similarly, since the average parenchymal thickness is 15–16 mm, and the typical shear wavelengths observed in this study were 20–35 mm, the wave propagation in the kidney was likely affected by the composite structural effects of the cortex and the medulla. Differentiating the wave propagation and mechanical properties of the cortex and medulla is an area of active investigation and may require increasing the imaging resolution (to 256^2–512^2), utilizing 3D MR techniques to acquire thinner slices (< 2 mm) to maintain approximately isotropic image resolution, and increasing the vibration frequency (> 200 Hz) to resolve structures with smaller wavelengths. The data here were analyzed using the 3×3×3 DI technique with directional filtering after calculating the curl of the wave field. Many other inversion techniques are available and are still the topic of active investigation.

The inherent detail of the Banff classification and scoring system is certainly advantageous as efforts continue to identify an imaging technique or combination of them that would correlate with pathology. One strategy which is being actively investigated involves evaluating other mechanical properties (such as poroviscoelasticity, anisotropy etc.) that may better refect pathology. Another strategy is to employ additional MRI techniques that have been used for assessment of KTxs, including diffusion-weighted imaging (DWI), blood oxygenation level dependent (BOLD) imaging, perfusion imaging, renal blood flow measurement (25–34). Perfusion imaging in animal studies has demonstrated the potential to provide information on transplant viability (34). All of these methods assess specific mechanical or physiological properties, but have limited validation in evaluation of renal transplants. More recent studies have begun to explore at least two “functional” imaging techniques at a time. For example, DWI has been investigated along with relaxation rate R2* values from BOLD imaging which demonstrate sensitivity for corticomedullary differentiation (29). This certainly raises the question of whether a combination of techniques might be the best approach to predict transplant viability including active (reversible) versus chronic (irreversible) changes.

Studies on diffusion tensor imaging elucidate imaging features of the microstructure of the renal parenchyma with reported excellent corticomedullary differentiation (35–38) and have noted directional differences in apparent diffusion coefficient measurements. In this study,

no data was collected to ascertain directionality effects on stiffness – ie, does stiffness change in relation to shear wave orientation relative to kidney axis? While preliminary studies have been performed on the liver, this has not been rigorously investigated in the kidneys and is a topic of active investigation.

MRE's in this study were done at different time points after transplantation, which could be another confounding factor. Perhaps the best study design would be to obtain baseline then serial measurements – fibrotic kidneys might have greater change from baseline. Additionally, to minimize any possibility of anastomotic dehiscence in this study, MRE was performed at least one-year after transplantation. MRE can likely be safely performed earlier, even months after transplantation. Non-invasively detecting early fibrosis prior to one-year may help to screen for those who are at risk for reduced graft function and survival and who may have a rejection-like gene expression signature (8).

Ultrasound elastography of KTxs (39–41) is appealing because it is relatively faster, less claustrophobic for some patients, and is available for patients where MRI is contraindicated. . The success of either ultrasound elastography or MRE will be in validation with pathology and being able to account for the factors that contribute to renal stiffness.

This investigation has shown that it is possible to apply MRE to evaluate the KTx. Ongoing investigation continues to ultimately ascertain if this new imaging biomarker can be used as a screening technique to quantitatively assess early inflammation and fibrosis in KTx's.

Acknowledgments

The authors acknowledge NIH grant EB001981. Special thanks to Wai Yee Lee, M.D. for his inspiration and steadfast belief in this work.

References

1. Racusen LC, Solez K, Colvin RB, et al. The Banff 97 working classification of renal allograft pathology. Kidney Int. 1999; 55(2):713–23. [PubMed: 9987096]
2. Schwarz A, Gwinner W, Hiss M, Radermacher J, Mengel M, Haller H. Safety and adequacy of renal transplant protocol biopsies. Am J Transplant. 2005; 5(8):1992–6. [PubMed: 15996250]
3. Preda A, Van Dijk LC, Van Oostaijen JA, Pattynama PM. Complication rate and diagnostic yield of 515 consecutive ultrasound-guided biopsies of renal allografts and native kidneys using a 14-gauge Biopty gun. Eur Radiol. 2003; 13(3):527–30. [PubMed: 12594555]
4. Patel MD, Phillips CJ, Young SW, et al. US-guided Renal Transplant Biopsy: Effi cacy of a Cortical Tangential Approach. Radiology 2010. 2010; 256:290–6.
5. Furness PN, Philpott CM, Chorbadjian MT, et al. Protocol biopsy of the stable renal transplant: a multicenter study of methods and complication rates. Transplantation. 2003; 76(6):969–73. [PubMed: 14508363]
6. Venkatesh SK, Yin M, Glockner JF, et al. MR elastography of liver tumors: preliminary results. AJR Am J Roentgenol. 2008; 190(6):1534–40. [PubMed: 18492904]
7. Domire ZJ, McCullough MB, Chen Q, An KN. Wave attenuation as a measure of muscle quality as measured by magnetic resonance elastography: initial results. J Biomech. 2009; 42(4):537–40. [PubMed: 19171346]
8. Park WD, Griffin MD, Cornell LD, Cosio FG, Stegall MD. Fibrosis with Inflammation at One Year Predicts Tranplant Functional Decline. J Am Soc Nephrol. 2010; 21:1–11. [PubMed: 20007749]
9. Yin M, Talwalkar JA, Glaser KJ, et al. Assessment of hepatic fibrosis with magnetic resonance elastography. Clin Gastroenterol Hepatol. 2007; 5(10):1207–13. e2. [PubMed: 17916548]
10. Chen J, Stanley D, KG, MY, PR, RE. Ergonomic Flexible Drivers for Hepatic MR Elastography. Book Ergonomic Flexible Drivers for Hepatic MR Elastography. City. 2010:1052.

11. Glaser K, Ehman RL. MR Elastography Inversions Without Phase Unwrapping. Book MR Elastography Inversions Without Phase Unwrapping. City. 2009:4669.
12. Manduca A, Lake DS, Kruse SA, Ehman RL. Spatio-temporal directional filtering for improved inversion of MR elastography images. Med Image Anal. 2003; 7(4):465–73. [PubMed: 14561551]
13. Solez K, Colvin RB, Racusen LC, et al. Banff '05 Meeting Report: differential diagnosis of chronic allograft injury and elimination of chronic allograft nephropathy ('CAN'). Am J Transplant. 2007; 7(3):518–26. [PubMed: 17352710]
14. Arani A, Plewes D, Krieger A, Chopra R. The feasibility of endorectal MR elastrography for prostate cancer localization. Magn Reson Med. 2011
15. Kolipaka A, McGee KP, Manduca A, Anavekar N, Ehman RL, Araoz PA. In vivo assessment of MR elastography-derived effective end-diastolic myocardial stiffness under different loading conditions. J Magn Reson Imaging. 2011; 33(5):1224–8. [PubMed: 21509882]
16. Li S, Chen M, Wang W, et al. A feasibility study of MR elastography in the diagnosis of prostate cancer at 3.0T. Acta Radiol. 2011; 52(3):254–8.
17. Mariappan YK, Glaser K, Hubmayr RD, Manduca A, Ehman RL, McGee KP. MR elastography of human lung parenchyma: Technical development, theoretical modeling and in vivo validation. J Magn Reson Imaging. 2011; 33(6):1351–61. [PubMed: 21591003]
18. Nedredal GI, Yin M, McKenzie T, et al. Portal hypertension correlates wih splenic stiffness as measured with MR elastography. J Magn Reson Imaging. 2011
19. Murphy MC, Glaser KJ, Manduca A, Felmlee JP, Huston J 3rd, Ehman RL. Analysis of time reduction methods for magnetic resonance elastography of the brain. Magn Reson Imaging. 2010; 28(10):1514–24. [PubMed: 20817440]
20. Granger JP. Pressure natriuresis: role of renal interstitial hydrostatic pressure. Hypertension. 1992; 19(suppl I):I-9–I-17. [PubMed: 1730460]
21. Granger JP, Scott JW. Effects of renal artery pressure on interstitial pressure and Na excretion during renal vasodilation. Am J Physiol. 1988; 255:F828–F33. [PubMed: 3189559]
22. Nakamura T, Sakamaki T, Kurashina T, Sato K, Ono Z, Marata K. Effect of Renal Perfusion Pressure on Renal Interstitial Hydrostatic Pressure and Sodium Excretion. Hypertension. 1995; 25:866–71. [PubMed: 7721445]
23. Warner L, Yin M, Glaser KJ, et al. Noninvasive In Vivo Assessment of Renal Tissue Elasticity During Graded Renal Ischemia Using MR Elastography. Investigative Radiology. 2011
24. Glodny B, Unterholzner V, Taferner B, et al. Normal kidney size and its influencing factors - a 64-slice MDCT study of 1.040 asymptomatic patients. BMC Urology. 2009; 9:19.10.1186/1471-2490-9-19 [PubMed: 20030823]
25. Blondin D, Lanzman RS, Mathys C, et al. Functional MRI of transplanted kidneys using diffusion-weighted imaging. Rofo. 2009; 181(12):1162–7. [PubMed: 19582653]
26. Eisenberger U, Thoeny HC, Binser T, et al. Evaluation of renal allograft function early after transplantation with diffusion-weighted MR imaging. Eur Radiol. 2010; 20(6):1374–83. [PubMed: 20013274]
27. Notohamiprodjo M, Reiser MF, Sourbron SP. Diffusion and perfusion of the kidney. Eur J Radiol. 2010; 76(3):337–47. [PubMed: 20580179]
28. Palmucci S, Mauro LA, Veroux P, et al. Magnetic resonance with diffusion-weighted imaging in the evaluation of transplanted kidneys: preliminary findings. Transplant Proc. 2011; 43(4):960–6. [PubMed: 21620026]
29. Thoeny HC, Zumstein D, Simon-Zoula S, et al. Functional evaluation of transplanted kidneys with diffusion-weighted and BOLD MR imaging: initial experience. Radiology. 2006; 241(3):812–21. [PubMed: 17114628]
30. Xu JJ, Xiao WB, Zhang L, Zhang MM. Value of diffusion-weighted MR imaging in diagnosis of acute rejection after renal transplantation. Zhejiang Da Xue Xue Bao Yi Xue Ban. 2010; 39(2): 163–7. [PubMed: 20387244]
31. de Priester JA, den Boer JA, Christiaans MH, et al. Automated quantitative evaluation of diseased and nondiseased renal transplants with MR renography. J Magn Reson Imaging. 2003; 17(1):95–103. [PubMed: 12500278]

32. de Priester JA, Kessels AG, Giele EL, et al. MR renography by semiautomated image analysis: performance in renal transplant recipients. J Magn Reson Imaging. 2001; 14(2):134–40. [PubMed: 11477671]
33. Sadowski EA, Djamali A, Wentland AL, et al. Blood oxygen level-dependent and perfusion magnetic resonance imaging: detecting differences in oxygen bioavailability and blood flow in transplanted kidneys. Magn Reson Imaging. 2010; 28(1):56–64. [PubMed: 19577402]
34. Wang JJ, Hendrich KS, Jackson EK, Ildstad ST, Williams DS, Ho C. Perfusion quantitation in transplanted rat kidney by MRI with arterial spin labeling. Kidney Int. 1998; 53(6):1783–91. [PubMed: 9607213]
35. Cutajar M, Clayden JD, Clark CA, Gordon I. Test-retest reliability and repeatability of renal diffusion tensor MRI in healthy subjects. Eur J Radiol. 2011
36. Gurses B, Kilickesmez O, Tasdelen N, Firat Z, Gurmen N. Diffusion tensor imaging of the kidney at 3 Tesla: normative values and repeatability of measurements in healthy volunteers. Diagn Interv Radiol. 2010
37. Kataoka M, Kido A, Yamamoto A, et al. Diffusion tensor imaging of kidneys with respiratory triggering: optimization of parameters to demonstrate anisotropic structures on fraction anisotropy maps. J Magn Reson Imaging. 2009; 29(3):736–44. [PubMed: 19243070]
38. Kido A, Kataoka M, Yamamoto A, et al. Diffusion tensor MRI of the kidney at 3.0 and 1.5 Tesla. Acta Radiol. 2010; 51(9):1059–63. [PubMed: 20735277]
39. Stock KF, Klein BS, Vo Cong MT, et al. ARFI-based tissue elasticity quantification in comparison to histology for the diagnosis of renal transplant fibrosis. Clin Hemorheol Microcirc. 2010; 46(2–3):139–48. [PubMed: 21135489]
40. Syversveen T, Brabrand K, Midtvedt K, et al. Assessment of renal allograft fibrosis by acoustic radiation force impulse quantification--a pilot study. Transpl Int. 2011; 24(1):100–5. [PubMed: 20819192]
41. Arndt R, Schmidt S, Loddenkemper C, et al. Noninvasive evaluation of renal allograft fibrosis by transient elastography – a pilot study. Transpl Int. 2010; 23:871–7. [PubMed: 20158692]

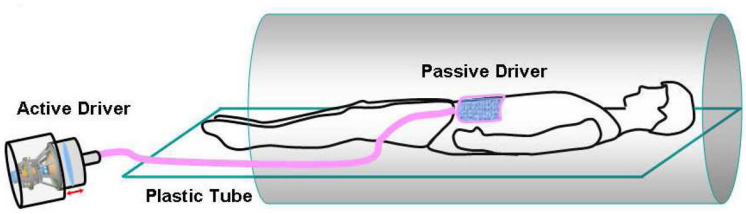

Figure 1. Diagram illustrating the MRE setup for evaluation of KTxs

The mechanical vibrations required for the MRE exams were supplied by an active driver system located outside of the scan room. The vibrations were conducted into the scanner bore via a plastic tube which terminated in a passive driver that was placed over the renal allograft.

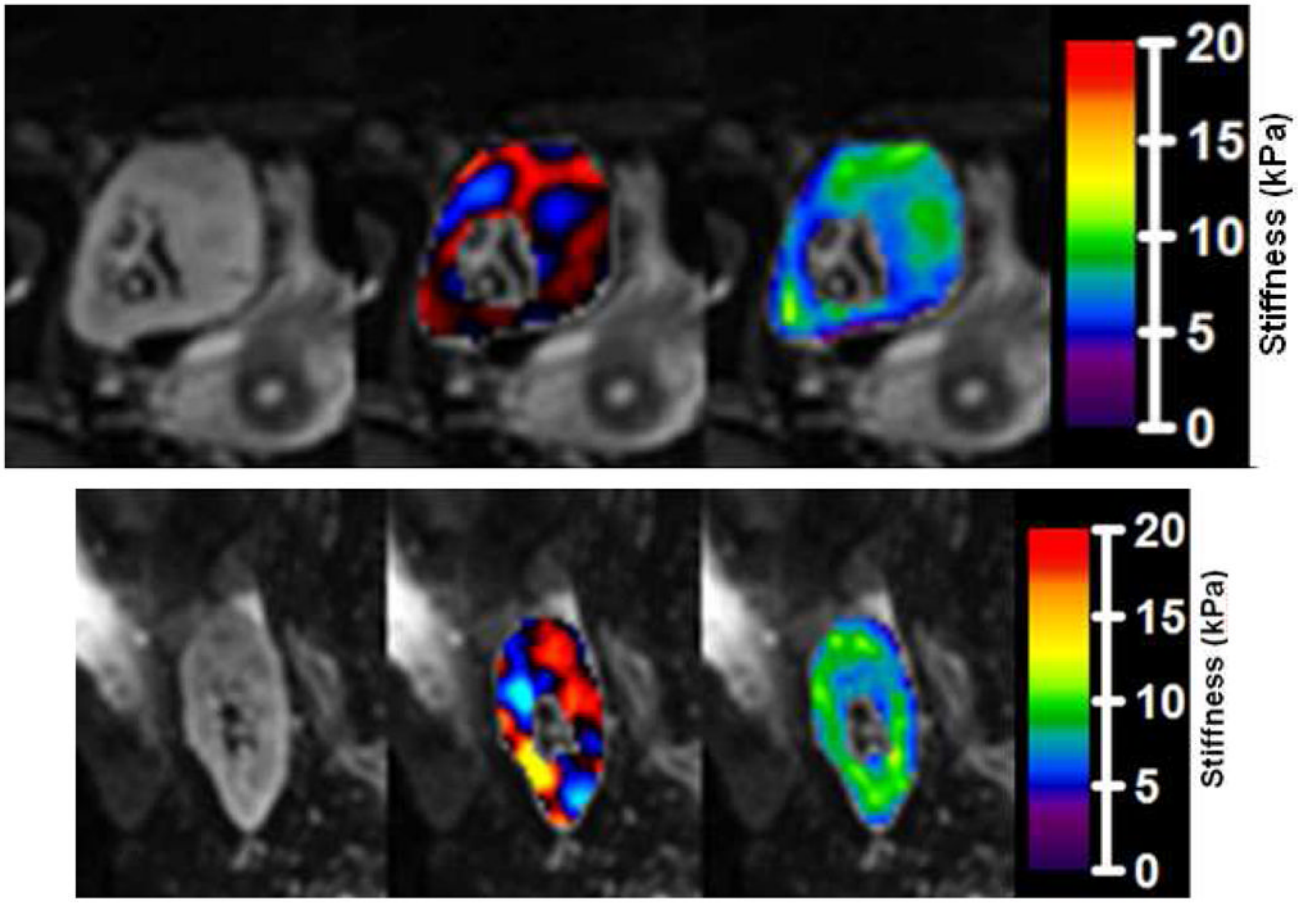

Figure 2. MRE acquisitions in the axial (a) and sagittal (b) planes

MRE results showing magnitude images from the MRE acquisition (left), fusion of the magnitude image with color-coded propagating shear waves in the kidney (middle), and fusion with color-coded calculated elastogram (right, in kPa).

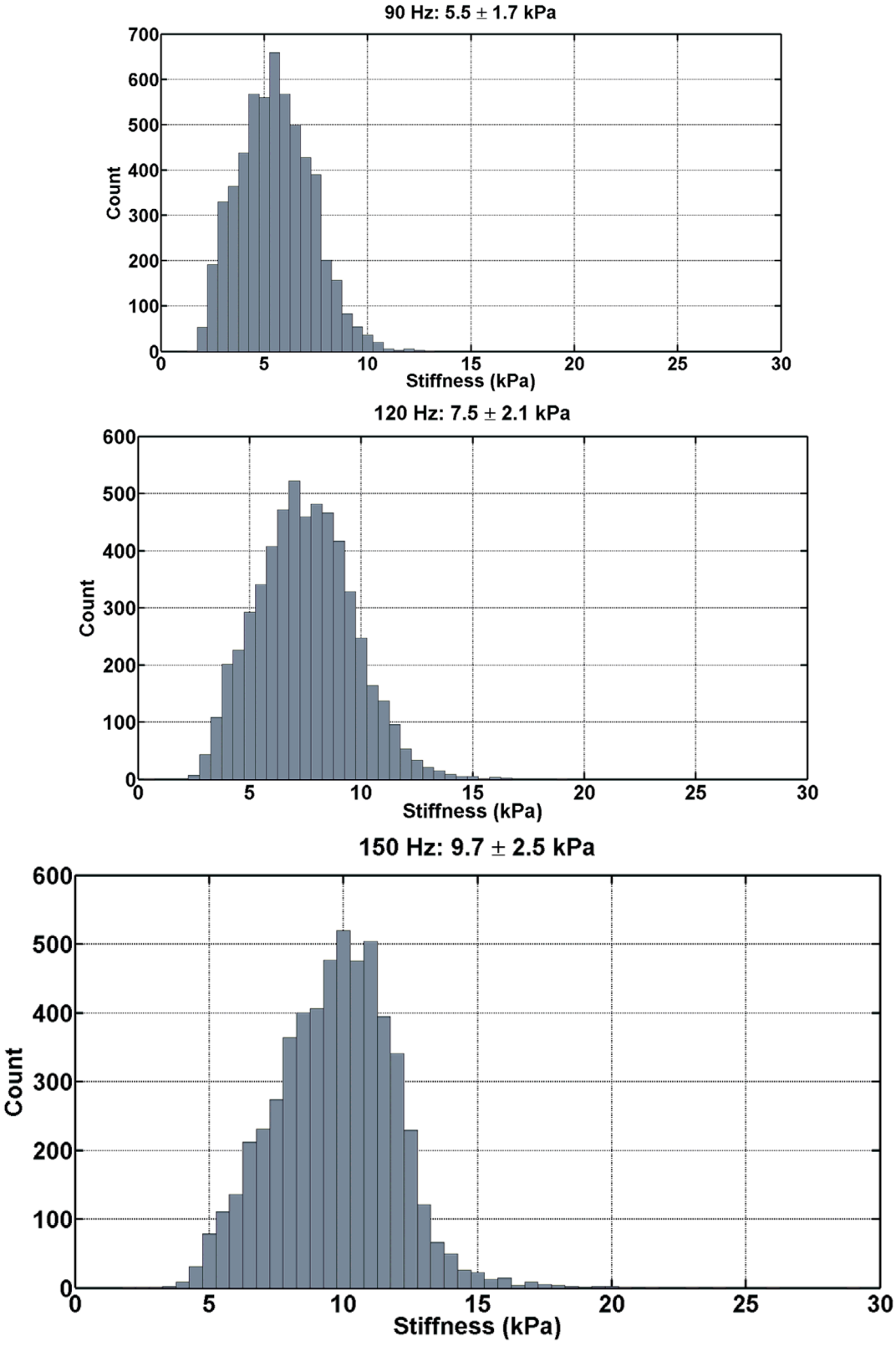

Figure 3. Histograms of the tissue stiffness (kPa) at 90 Hz (a), 120 Hz (b), and 150 Hz (c) for one patient

These tissue stiffness values were obtained from the segmented volume of non-hilar renal parenchyma. At 90 Hz, the mean tissue stiffness was 5.5 ± 1.7 kPa; at 120 Hz, the mean tissue stiffness was 7.5 ± 2.1 kPa; and, at 150 Hz, the mean tissue stiffness was 9.7 ± 2.5 kPa.

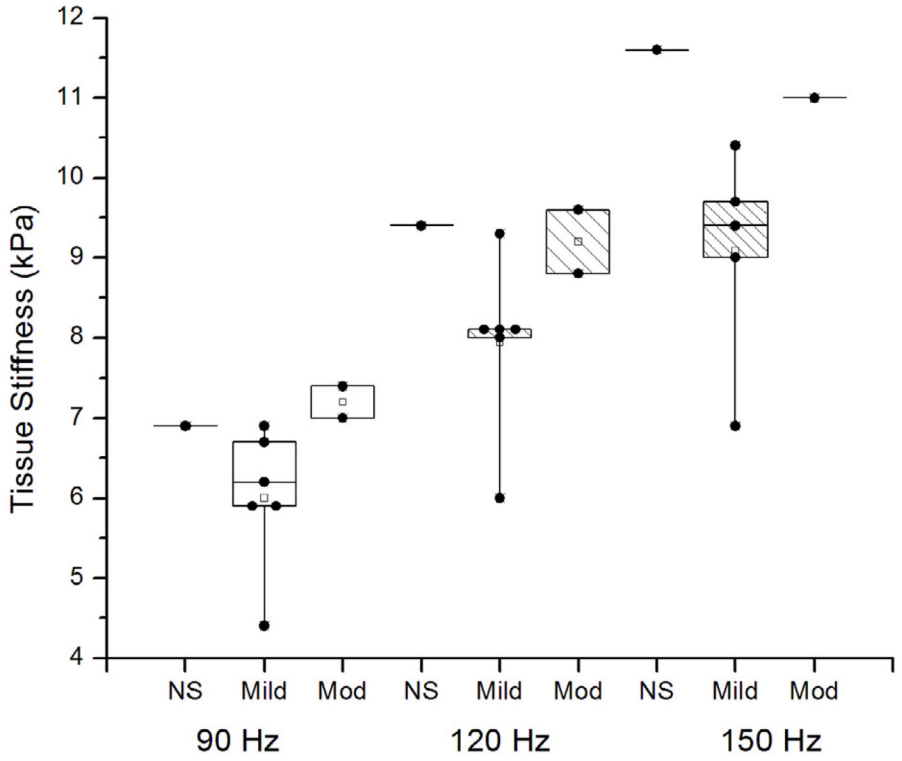

Figure 4. Boxplots of mean tissue stiffness at all the frequencies of vibration (90 Hz, 120 Hz, and 150 Hz) corresponding to the pathology results ("NS" No significant fibrosis), "Mild" fibrosis, and "Mod" (Moderate) fibrosis)

The individual data points (●) have been superimposed over the boxplots. The mean tissue stiffness was greater with moderate fibrosis than mild fibrosis. There was some overlap in the range of stiffness values between moderate and mild fibrosis at 120 Hz. At all three frequencies, there was no significant difference between mean stiffness values associated with mild versus no significant fibrosis.

Table 1

Patient Characteristics.

Patient	Age/Sex	Transplant	History		eGFR[a]	BP
1	31 M	1st transplant Living-related	**1**	IgA nephropathy	44	103/69
			2	History of Banff 1A acute rejection		
			3	Here for 5-year protocol biopsy		
2	53 M	1st transplant Living-unrelated	**1**	IgA nephropathy with focal segmental glomerulosclerosis; recurrent IgA nephropathy	58	123/79
			2	Here for 2-year protocol biopsy		
3	63 F	1st transplant Living donor	**1**	Radiation nephritis secondary to treatment for retroperitoneal leiomyosarcoma	45	117/69
			2	Here for 5-year protocol biopsy.		
4	40 M	4th transplant Deceased donor	**1**	Congenital solitary kidney with hypoplasia	27	124/87
			2	Here for 5-year protocol biopsy.		
5	56 M	1st transplant Living donor	**1**	Membranous nephropathy with subclinical recurrence	25	126/84
6	55 M	1st transplant Living related	**1**	IgA nephropathy	53	136/81
			2	Here for 1-year protocol biopsy		
7	58 F	1st transplant Living donor	**1**	PCKD	46	142/77
			2	Bilateral nephrectomies		
			3	Here for 2-year protocol biopsy		
8	31 F	1st transplant Living related	**1**	Vesicoureteral reflux and chronic pyelonephritis	31	102/67
			2	Bilateral nephrectomies		
			3	Here for 5-year protocol biopsy		
9	33 F	1st transplant Living related	**1**	MPGN[b]	26	115/77
			2	Recurrent MPGN and transplant glomerulonephropathy since transplant		
			3	Here for 4-year biopsy		
10	71 M	1st transplant Living related	**1**	Endstage renal failure due to diabetes mellitus type 2 and hypertension	27	128/61

Patient	Age/Sex	Transplant	History	eGFR[a]	BP
			2 Here for 2-year protocol biopsy		

The most common etiology for renal failure requiring transplantation was proliferative glomerulonephritis (4/10 patients). One patient (Patient #4) had had multiple transplants; the others still had their initial transplant. One patient was here for the first annual protocol biopsy; four patients for the 2-year protocol biopsy; one patient for a 4-year post-transplant biopsy; and, four patients for the 5-year protocol biopsy.

a: (ml/min/1.73m^2),

b: Membranoproliferative glomerulonephritis

Table 2

Pathology.

Patient	Pathology Diagnosis	Banff Classification and Scoring											
		g	i	t	v	ah	cg	ci	ct	cv	mm	ptc	c4d
1	**Mild** interstitial fibrosis; patchy tubular atrophy	0	0	0	0	2	0	1	1	1	1	0	0
2	**Mod** interstitial fibrosis; tubular atrophy	0	1–2	0	0	0	2	2	2	2	1	0	0
3	**Inadequate** biopsy sample consisting of mostly renal medulla. (on LM comment, tubules showed no significant interstitial changes)	na	na	na	na	na	na	na	na	na	na	na	na
4	**Mod** interstitial fibrosis; tubular atrophy >30% cortex	2	0	0	0	3	2	2	2	1	0	3	0
5	**Mild** interstitial fibrosis and tubular atrophy	0	0	0	0	0	0	0	1	1	0	0	0
6	**Mild** interstitial fibrosis and tubular atrophy; (additional comment: borderline cellular rejection except severe tubulitis in inflamed area)	0	1	3	0	0	0	1	0	0	NR[a]	0	0
7	**No significant** interstitial fibrosis or tubular atrophy; minimal focal inflammation	0	0	0	0	0	0	0	0	0	NR	0	NR
8	**Mild** interstitial fibrosis and tubular atrophy	0	0	0	0	1	0	1	1	2	0	0	NR
9	**Mild** tubular atrophy and interstitial fibrosis (15% cortex)	0	0	0	0	2	3	1	1	2	NR	0	0
10	**Mild** interstitial fibrosis and tubular atrophy.	0	0	0	0	0	0	1	1	1	NR	0	NR

Pathology reports including the Banff scores yielded six patients with a diagnosis of mild interstitial fibrosis, two patients with moderate (mod) interstitial fibrosis, one patient with no significant intersitial fibrosis, and one patient with an inadequate tissue specimen for pathological evaluation (na). Some of the Banff scores were not directly reported in the pathology report and are noted ([a]NR not reported). Banff scoring provides quantitative criteria for early type of allograft glomerulitis (g), mononuclear cell interstitial inflammation (i), tubulitis (t), intimal arteritis (v), arteriolar hyaline thickening (ah), allograft glomerulopathy (cg), interstitial fibrosis (ci), tubular atrophy (ct), fibrous intimal thickening (cv), mesangial matrix increase (mm), peritubular capillaries (ptc), and c4d and/or immunoglobulin in peritubular capillaries (c4d) (10).

Table 3a

Tissue stiffness values for each patient at 90 Hz, 120 Hz, and 150 Hz vibration.

Fibrosis	Patient #	Renal Tissue Stiffness (kPa)					
		at 90 Hz		at 120 Hz		at 150 Hz	
NS	7	6.9	mean 6.9	9.4	mean 9.4	11.6	mean 11.6
Mild	1	6.7	6.0	8.1	7.9*	NA	9.1*
	5	6.2		8.1		9.7	
	6	6.9		9.3		10.4	
	8	4.4		6.0		6.9	
	9	5.9		8.0		9.0	
	10	5.9		8.1		9.4	
Mod	2	7.4	7.2	9.6	9.2	NA	11.0
	4	7.0		8.8		11.0	
Non-Dx	3	6.4	6.4	8.5	8.5	12	12

*Significant difference between mean stiffness values of mild and no significant fibrosis ($p<0.05$).

Table 3b

Repeatability results for Patient #5 returning 22 months later.

Repeatability Results	Renal Tissue Stiffness (kPa)			
	at 90 Hz	at 120 Hz	at 150 Hz	
MRE #1	5.2 ± 1.9	7.0 ± 2.3	8.9 ± 2.9	(8.9 ± 2.3)
MRE #2	5.5 ± 1.7	7.5 ± 2.1	9.7 ± 2.5	(9.7 ±− 2.2)
MRE #3	5.4 ± 1.7	7.3 ± 4.5	9.5 ± 36.2[§]	(8.8 ± 2.1)
mean	5.4	7.3	9.4	(9.1)
sd	0.2	0.3	0.4	(0.5)
COV	2.9%	3.5%	4.4%	(5.4%)

[§]Large standard deviation is due to spikes (outliers) in the elastogram. Since the median is a more robust measure of the central value in this case, we parenthetically report the “trimmed mean and standard deviation.” Data more than three standard deviations above or below the median of the original ROI data were removed to exclude outliers while maintaining 99.7% of the original data, and then the mean and standard deviation of the remaining data were reported. This methodology was also performed for the other data which did not have significant outliers, and as expected, the other data were minimally affected.

Tissue stiffness values were determined using a 3×3×3 DI DF algorithm. Level of pathological fibrosis (NS: no significant fibrosis; Mild: mild fibrosis; Mod: moderate fibrosis; Non-Dx: non-diagnostic) based on Banff criteria is noted for each patient (Table 3a). MRE at 150 Hz vibrations was not performed on the first two patients in the study (denoted by “NA.”). MRE was repeated three times with complete disassembly and reassembly of the MRE apparatus between each repetition for Patient #5 who returned for clinical follow-up 22 months later (Table 3b).